Technical University of Denmark

A Modified TSD Specimen for Fracture Toughness Characterization – Fracture Mechanics Analysis and Design

Berggreen, Christian; Carlsson, Leif A.

DTU Library
Technical Information Center of Denmark

Journal of Composite Materials

http://jcm.sagepub.com/

Published by:

$SAGE

http://www.sagepublications.com

On behalf of:

American Society for Composites

A Modified TSD Specimen for Fracture Toughness Characterization − Fracture Mechanics Analysis and Design

CHRISTIAN BERGGREEN*

Department of Mechanical Engineering, Technical University of Denmark
Nils Koppels Allé, Building 403, DK-2800 Kgs. Lyngby, Denmark

LEIF A. CARLSSON

Department of Mechanical Engineering, Florida Atlantic University, 777 Glades Road
Boca Raton, FL 33431, USA

ABSTRACT: The tilted sandwich debond (TSD) specimen has been recognized as a viable candidate for characterization of the face/core fracture resistance. Analysis, however, shows that the range of phase angles that can be realized by altering the tilt angle and other parameters of the test is quite limited. A method to extend the range of mode-mixities of the TSD specimen is to introduce a larger amount of transverse shear by reinforcing the loaded upper face with a stiff metal plate. Analysis shows that this method extends the range of phase angles to a practically useful range. Guidelines on selection of thicknesses of the reinforcement, and design considerations for further modifications are provided.

KEY WORDS: sandwich structures, fracture mechanics, interfaces, mixed mode loading.

INTRODUCTION

THE TILTED SANDWICH debond (TSD) specimen, shown in Figure 1, was introduced as a debond test for foam cored sandwich specimens in 1999 by Li and Carlsson [1]. The specimen is tilted which means that the debonded face will be subject to an axial load, P_A, as in Figure 1, in addition to the normal load, P_N ($P_A = P\sin\theta$, $P_N = P\cos\theta$). The axial load was initially thought to promote a negative shear stress at the crack tip that would mitigate the shear stress due to the bimaterial interface and counter the tendency for the crack to kink down into the core (Figure 2). Testing of foam cored sandwich specimens, however, showed that the crack initially kinked down into the core (although the crack returned to the upper face/core interface as the crack propagated further) [1]. Experimental tests on sandwich specimens with a certain combination of face and core

---
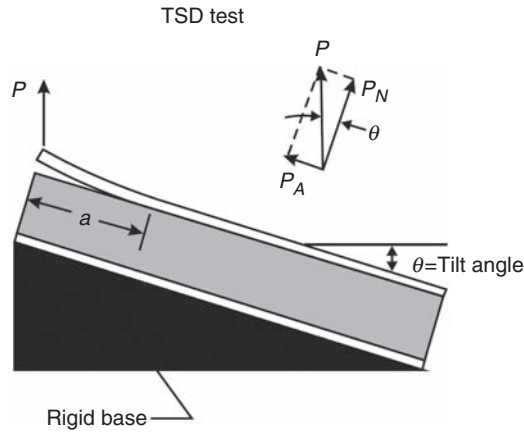
Figure 1. *Schematic representation of the conventional TSD specimen.*
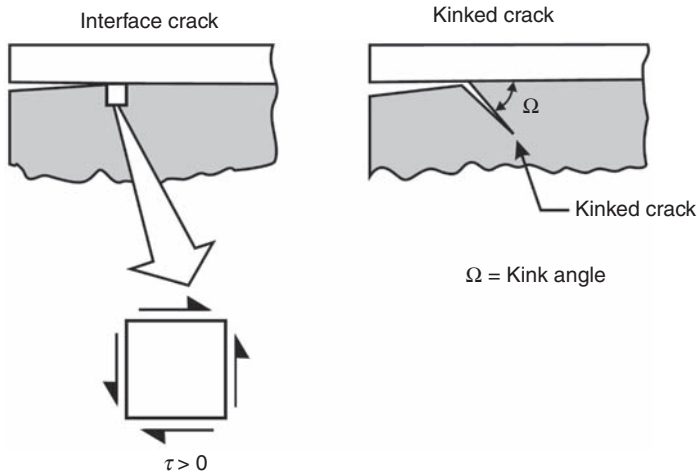
Figure 2. *Illustration of crack kinking into the core under positive shear at the crack tip.*

materials have been conducted at different tilt angles, but the results reveal that the fracture resistance curves (*R*-curves) are very similar. Subsequent analysis [2] confirmed that the mode-mixity for a typical TSD specimen remains quite unaffected by the tilt angle.

It is generally recognized that the fracture toughness for propagation of an interface crack between two dissimilar materials depends on the mode-mixity often expressed as a 'phase angle', ψ, where ψ quantifies the amount of mode II dominated loading of the crack and the direction of shear. It should be pointed out that positive shear stress ahead of the crack tip, $\psi > 0$, see Figure 2, tends to promote kinking of the crack into the core [3,4]. Conversely, zero or a negative shear stress, $\psi < 0$, will generally promote interface growth, although cases have been reported where negative shear leads to crack kinking into the face sheet [5,6]. The face sheets in the specimens examined by Berggreen et al. [5] and Lundsgaard-Larsen et al. [6] were composite laminates. Kinking into the face sheet is not physically possible for metal faces.

A full characterization of debond failure thus requires testing over a wide range of mode-mixities. Only a limited number of test fixtures incorporates the possibility for a direct specification of the mode-mixity applied during the test. A very intriguing test method is the double cantilever beam test with uneven bending moments (DCB-UBM), devised by Sørensen et al. [7] for monolithic composites where the ends of a DCB specimen are loaded by moments. The directions of the moments and their relative magnitudes can be varied, allowing for a large range of mode-mixities. This test was applied on sandwich specimens by Østergaard et al. [8] and Lundsgaard-Larsen et al. [9]. This method produces stable crack growth if run under displacement control since the crack loading does not change with crack length, making the DCB-UBM specimen highly attractive for measurement of interface cohesive laws, where a stable crack growth is required in order to reach a fully developed process zone behind the crack tip. Unfortunately, the test method requires a quite complicated test rig and tall test frame and for sandwich specimens also ultra-high strength steel reinforcements of the face sheets. Thus, it may not be easily applied.

Recently the classic mixed mode bending (MMB) test [10,11] developed for delamination testing of monolithic composite specimens was modified to also incorporate sandwich specimens [12,13]. Although the sandwich MMB test fixture is much less complicated to prepare and use than the DCB-UBM and the specimen does not need to be reinforced, the range of mode-mixities possible for one specimen geometry, through the adjustment of the lever arm distance in the fixture, is more limited.

The characterization of delaminations in composite laminates and debonds in layered materials typically utilizes layered beam specimens with a pre-crack at the interface. Analysis of such specimens has traditionally been focused on a combination of axial loads and pure moments acting on cross sections away from the crack tip region. For shorter crack lengths, however, transverse shear is known to affect the energy release rate of such specimens, and analysis by Li et al. [14] and Ferrie et al. [15] reveals that shear will also change the phase angle, ψ. The shear force will cause rotation of the region close to the crack tip, 'root rotation', in excess of the rotation due to the average transverse shear strain.

For the TSD geometry, it seems plausible that a way to enhance the shear loading is to use a thicker face or a steel plate reinforced face. From a practical point of view it is difficult to increase the face thickness just for testing purposes. The most viable option to increase the shear force is to adhesively bond a steel bar to the upper face.

In this article, the reinforced TSD specimen will be examined using detailed finite element analysis. Further modifications are also examined.

SOLUTIONS FOR INTERFACE CRACKS

Linear-elastic fracture mechanics for debonding of layered materials has been considered by several authors, see the extensive review provided by Hutchinson and Suo [16]. A 'TSD like' specimen was considered, see Figure 3. The configuration shown in Figure 3 is representative for a long TSD specimen with a very thick core and a thin face sheet subject to an axial edge load and edge moment[1] at long crack lengths. The solution for the stress

---

[1]The shear loading due to the transverse load component at the edge is neglected here, and its action is replaced by the moment, M.
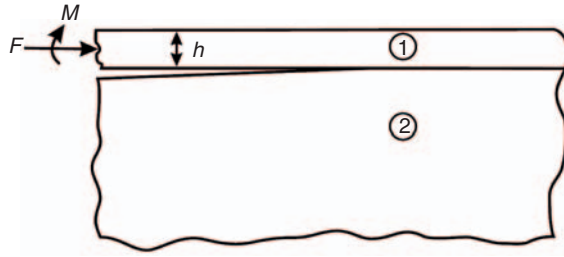
Figure 3. *Face sheet (1) subject to edge loads supported by an infinite core (2).*
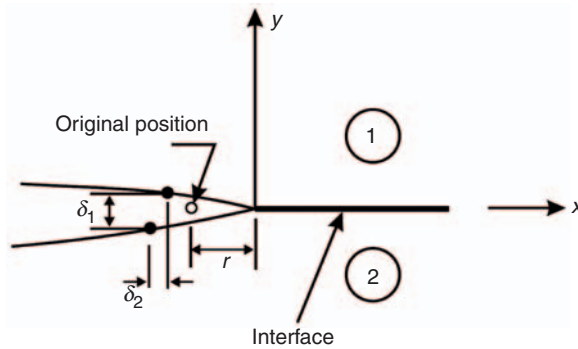
Figure 4. *Crack flack displacements. Open circle: point on the crack faces before loading. Filled circles: Position of point after loading.*

intensity factors for this specific geometry and loading may be extracted from the general analysis of beam-like specimens presented by Hutchinson and Suo [16].

$$K_1 + iK_2 = h_f^{-i\varepsilon}\left(\frac{1-\alpha}{1-\beta^2}\right)^{1/2}\frac{1}{\sqrt{2}}\left(Fh_f^{-1/2} - i2\sqrt{3}Mh_f^{-3/2}\right)e^{i\omega}, \tag{1}$$

where $i = \sqrt{-1}$, K_1 and K_2 are 'components' of the complex stress intensity factor, and h_f is the face sheet thickness. F and M are edge force and moment acting on the debonded face sheet, respectively. ε is the oscillatory index given for isotropic materials by:

$$\varepsilon = \frac{1}{2\pi}\ln\left(\frac{1-\beta}{1+\beta}\right), \tag{2}$$

where β is a bimaterial interface constant (Dundurs parameter [17]) given by:

$$\beta = \frac{1}{2}\frac{G_1(1-2v_2) - G_2(1-2v_1)}{G_1(1-v_2) + G_2(1-v_1)}, \tag{3}$$

where G_i ($i = 1,2$) represents the shear moduli of materials 1 and 2 above and below the interface, Figure 4. The parameter α is given by:

$$\alpha = \frac{\bar{E}_1 - \bar{E}_2}{\bar{E}_1 + \bar{E}_2}, \tag{4}$$

where $\bar{E} = E$ and $E/(1 - v^2)$ for plane stress and plane strain, respectively, and where E and v are Young's modulus and Poisson's ratio, respectively. The parameters α and β are called 'mismatch' parameters after their derivation by Dundurs [17]. Hence, if both materials across the interface are the same, there is no mismatch and $\alpha = \beta = 0$.

The parameter ω in Equation (1), is a phase angle that depends on the bimaterial parameters α and β, and assumes a value of 52.1° for a homogeneous isotropic specimen [16].

For the purpose of determining stress intensity factors based on finite element analysis, it is desirable to utilize displacements of the crack surfaces behind the crack tip. Figure 4 illustrates schematically how a point on the crack faces, originally at a distance, r, behind the tip, displaces upon loading, with opening (δ_1) and sliding (δ_2) displacements. The definitions of δ_1, and δ_2 shown in Figure 4 are consistent with positive opening and shear stresses, σ_y and τ_{xy}, in front of the crack tip. Hutchinson and Suo [16] provide the following expression for the displacements:

$$\delta_2 + i\delta_1 = \frac{8(K_1 + K_2)(1 - \beta^2)^{1/2}}{(1 + 2i\varepsilon)E^*}\left(\frac{r}{2\pi}\right)r^{i\varepsilon}. \tag{5}$$

The energy release rate available for interface crack growth is [16]:

$$G = \frac{(1 - \beta^2)}{E^*}\left(K_1^2 + K_2^2\right), \tag{6}$$

where

$$\frac{1}{E^*} = \frac{1}{2}\left(\frac{1}{E_1} + \frac{1}{E_2}\right). \tag{7}$$

Expressions for the crack-tip stress field are given by Hutchinson and Suo [16].

It is widely recognized that in most cases the stress oscillation and contact occur in an extremely narrow region behind the crack tip. Further, it is common practice to suppress the oscillating singularity by letting $\alpha = \beta = 0$ in the expression (1) for the stress intensity factors. With $\alpha = \beta = 0$, K_1 and K_2 mathematically retain their conventional meaning as measures of the intensities of the tensile and shear stress fields ahead of the crack tip, that is, $K = K_I + i K_{II}$. In this article the TSD specimen will be examined using both complex and conventional stress intensity factors, and from here on designated as the 'full' and 'reduced' formulation indicated by 'F' and 'R', respectively. For the reduced formulation $(\varepsilon = 0)$, the displacements, δ_1 and δ_2, Equation (5) become:

$$\delta_2 + i\delta_1 = \frac{8}{E^*}(K_1 + iK_{II})\left(\frac{r}{2\pi}\right). \tag{8}$$

Furthermore, the expressions for phase angle, ψ, for the $\varepsilon \neq 0$ and $\varepsilon = 0$ definitions become,

$$\psi_F = \tan^{-1}\left(\frac{\text{Im}[Kl^{i\varepsilon}]}{\text{Re}[Kl^{i\varepsilon}]}\right), \tag{9a}$$

$$\psi_R = \tan^{-1}\left(\frac{K_{II}}{K_I}\right), \tag{9b}$$

where l in Equation (9a) is defined as the characteristic length of the crack problem. For sandwich debond problems the characteristic length is often arbitrarily chosen as the face thickness. The selection of the length l will be discussed further later.

TSD Analysis

By neglecting the effects of shear on the crack tip stress and displacement field, it is possible to model the TSD specimen, Figure 1, using Equation (1) with:

$$F = -P\sin\theta, \tag{10a}$$

$$M = Pa\cos\theta, \tag{10b}$$

where P is the vertical force and θ is the tilt angle, see Figure 1. For the reduced formulation ($\varepsilon = \beta = 0$), and $e^{i\omega} = \cos\omega + i\sin\omega$, Equations (1) and (10) yield,

$$K_{\mathrm{I}} = \sqrt{\frac{1-a}{2h_f}}\left(-\sin\theta\cos\omega + 2\sqrt{3}\left(\frac{a}{h_f}\right)\cos\theta\sin\omega\right)P, \tag{11a}$$

$$K_{\mathrm{II}} = \sqrt{\frac{1-a}{2h_f}}\left(-\sin\theta\sin\omega - 2\sqrt{3}\left(\frac{a}{h_f}\right)\cos\theta\cos\omega\right)P. \tag{11b}$$

For a TSD specimen with a thin face sheet and a long crack it is noted from Equations (11) that the second terms in the expressions for K_{I} and K_{II} will dominate. Hence, the phase angle, ψ_R, will become independent of crack length, face sheet thickness and tilt angle,

$$\psi_R = \tan^{-1}\left(\frac{K_{\mathrm{II}}}{K_{\mathrm{I}}}\right) = -\tan^{-1}(\cot\omega) = \omega - 90°. \tag{12}$$

Furthermore, for a homogeneous TSD specimen, $\omega = 52.1°$ [16]. Hence, for this case the phase angle becomes: $\psi_R = -37.9°$. For bimaterial specimens, Hutchinson and Suo [16] provides results for the angle ω in graphical form over the range ($-0.8 \leq \alpha \leq 0.8$). Unfortunately, this range does not include typical sandwich material configurations where the mismatch in material properties across the face/core interface is extreme ($\alpha \approx 1$). From the analysis in Hutchinson and Suo [16] it can be noted that ω is increasing when α is increasing (larger bimaterial mismatch), which will produce a more mode I dominated crack loading. For shorter crack lengths, however, it is not appropriate to replace the edge moment, M, in Equation (1) with the 'statically equivalent' normal force component ($P\cos\theta$) times the crack length (a) as in Equation (10b), because the transverse shear force becomes more significant [14]. This will here be examined using finite element analysis.

PARAMETRIC FRACTURE ANALYSIS

A potential method to increase the range of mode-mixities is to reinforce the upper face with a steel bar, see Figure 5. The effect of stiffening of the loaded face sheet on the phase angle is investigated using detailed finite element analysis. The parameters that will be varied are the reinforcement thickness, h_s, and the tilt angle, θ. The basic sandwich geometry investigated consists of 2 mm face sheets made from E-glass woven rovings and epoxy
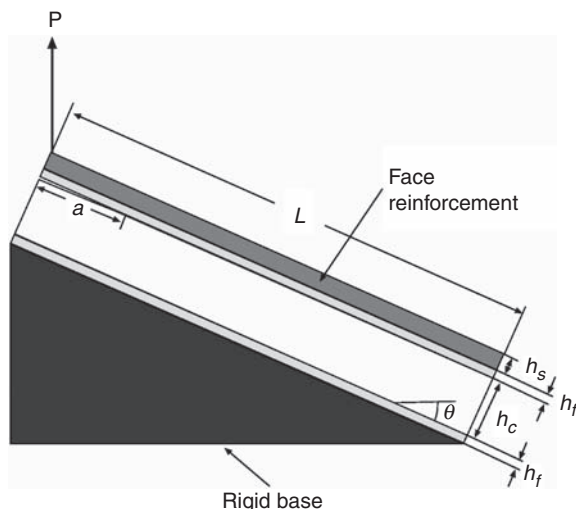
Figure 5. *Schematic representation of the reinforced TSD specimen.*

Table 1. *Geometrical properties in the parametric analysis.*

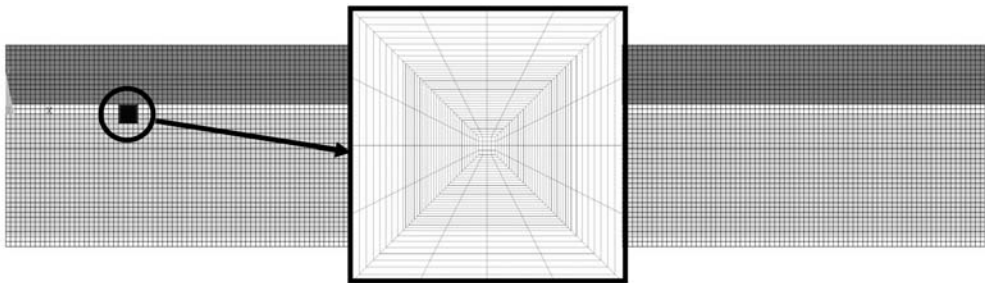| Geometrical properties		
Specimen length (mm)	L	200
Face thickness (mm)	h_f	2, 4
Core thickness (mm)	h_c	5, 10, 25, 50, 100
Crack length (mm)	a	25, 50
Reinforcement thicknesses (mm)	h_s	1, 2, 4, 8, 12
Tilt angle (°)	θ	−85, −75, −60, −30, 0, 30, 60, 75, 85

resin and 25 mm thick Divinycell H45, H100, and H200 foam cores. The (steel) reinforcement is considered adhesively bonded to the upper face sheet. Furthermore, in order to enhance the effect of the transverse shear a short crack length (25 mm) relative to the specimen length (200 mm) is chosen. Geometrical and mechanical properties considered in the parametric analysis can be found in Tables 1 and 2.

In order to determine fracture mechanical properties, that is, energy release rate and phase angle, for the various configurations of the modified TSD specimen, the crack surface displacement extrapolation (CSDE) method based on relative crack flank displacements was applied combined with a calculation of the J-integral. The CSDE-method was presented earlier by Berggreen et al. [5] in combination with a 2D finite element model similar to the one used herein. Expressions for the energy release rate and phase angle can also be found in Berggreen et al. [5].

The finite element model consists of 4- and 8-noded iso-parametric plane elements. In order to accurately capture the relative crack flank displacements near the tip, see Figure 4, a highly densified mesh was used in the region surrounding the crack tip. Furthermore, the dense mesh region is divided into element rings and used for several J-integral calculations which are then averaged and compared with the energy release rate determined from the

Table 2. Mechanical properties of face, core, and steel.

Mechanical properties

Face (GFRP, CFRP)			Cores (H45, H100, H200)		
In-plane Young's moduli (GPa)	$E_1,$ E_2	20.6 44.0	Young's modulus (MPa)	E_c	55 130 250
Out-of-plane Young's modulus (GPa)	E_3	9.90 9.90	Shear modulus (MPa)	G_c	15 35 85
In-plane shear modulus (GPa)	G_{12}	3.10 6.62	Poisson's ratio (—)	v_c	0.32 0.32 0.32
Out-of-plane shear moduli (GPa)	$G_{13},$ G_{23}	2.90 6.20	Steel reinforcement		
In-plane Poisson's ratios (—)	v_{12}	0.12 0.12	Young's modulus (GPa)	E_s	210
Out-of-plance Poission's ratios (—)	$v_{13},$ v_{23}	0.37 0.37	Poission's ratio (—)	v_s	0.3

Figure 6. *Finite element mesh applied in parametric analysis of the reinforced TSD specimen ($h_r = 12\,mm$). (a) global mesh and (b) near tip mesh region. Minimum element size is 3.33 μm.*

relative crack flank displacements and using the CSDE-method. The finite element mesh is shown in Figure 6.

The TSD simulation is conducted by restricting all DOF's at the bottom surface of the lower face sheet. Axial, P_A, and normal, P_N, loads are applied at the upper left corner of the reinforcement layer according to the tilt angle, θ,

$$P_A = P \sin \theta, \tag{13a}$$

$$P_N = P \cos \theta. \tag{13b}$$

The finite element analysis is geometrically linear. For each specimen configuration, the load is applied corresponding to an energy release rate level $G = G_{IC}$ of the foam core. G_{IC} for the H45, H100, and H200 foams are about 200, 400, and 800 J/m^2 [18].
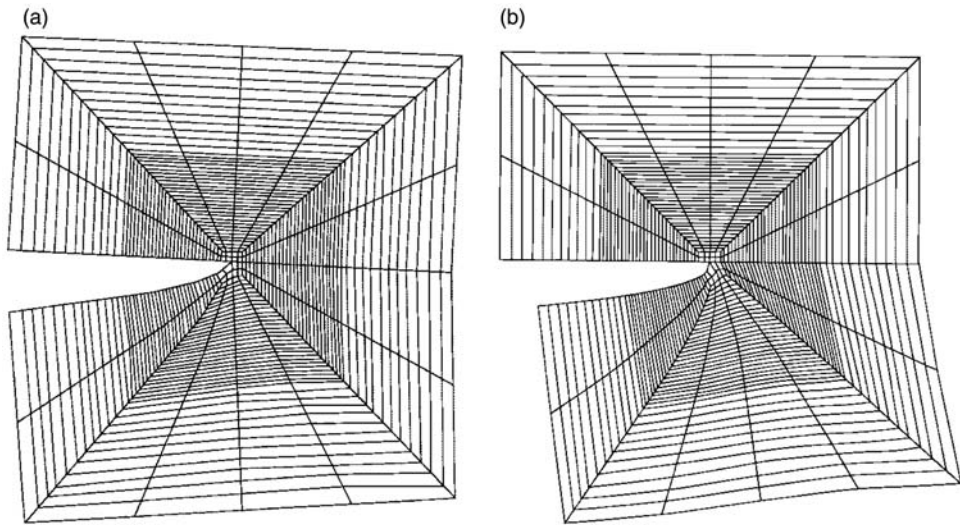
Figure 7 shows the phase angle for the TSD specimens with H45, H100, and H200 cores calculated according to the reduced formulation ($\varepsilon = 0$) as a function of the tilt angle for
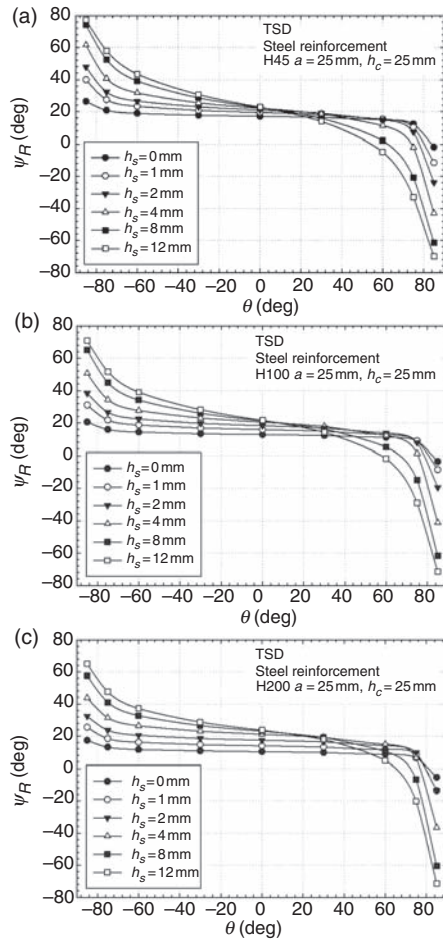
Figure 7. *Phase angle (reduced formulation) as function of tilt angle for a reinforced TSD specimen. (a) H45, (b) H100, and (c) H200 core cases.*

various reinforcement thicknesses. For the unreinforced ($h_s = 0$) original TSD specimen with a given core the phase angle is almost constant over the range of tilt angles between $\{-75° < \theta < 75°\}$, confirming the earlier analyses and testing by Li and Carlsson [2]. However, Figure 7 shows also that by reinforcing the upper face sheet with a stiff steel layer the range of phase angles is expanded. For a H100 core and a reinforcement thickness of 12 mm (Figure 7(b)), the phase angle assumes values between $\psi_R = \pm 70°$ over the range of tilt angles, θ, from $-85°$ to $85°$. The results for the specimens with H45 and H200 cores are similar, see Figure 7(a) and (c).

As indicated earlier, the increased range of phase angles can be associated with the increased shear loading and crack tip root rotation when the reinforcement layer thickness, h_s, is increased. Deformed crack tip meshes for a TSD specimen with a H100 core without and with 12 mm steel reinforcement are shown in Figure 8 ($\theta = 75°$). Significant root rotation is clearly observed for the reinforced TSD-specimen in accordance with the

Figure 8. Crack tip deformations at $\theta = 75°$ for a specimen with a H100 core. (a) Original TSD specimen and (b) reinforced TSD specimen, ($h_s = 12$ mm).

analysis of Li et al. [14]. The phase angles for the unreinforced and reinforced specimens are: $\psi_R = 8.89°$ and $\psi_R = -29.12°$. The crack tip rotation apparently contributes to the increasing amount of negative mode-mixity.

Further inspection of the results in Figure 7 reveals that unreinforced TSD specimens display positive phase angles for tilt angles up to around $\theta = 80°$ for all core materials, indicating that crack kinking into the core is likely. It was mentioned earlier that a TSD specimen made from a single material loaded at zero tilt angle ($\theta = 0$) has a negative phase angle ($\psi_R = -38°$). It was also pointed out that the bimaterial character of the specimen will shift the mode-mixity towards mode I. For the sandwich configuration considered here, the mismatch is extreme ($\alpha \approx 1.0$) and the phase angles are indeed shifted towards mode I dominance, in agreement with the trends predicted from simplified, earlier discussed analysis of the TSD specimen. As shown in Figure 7, a way to counteract this tendency is to reinforce the face sheet. Relatively thick reinforcements ($h_s = 8$ and 12 mm) are most effective.

Both unreinforced and reinforced TSD specimens are prone to kinking at negative and small positive tilt angles according to Figure 7. So far the discussion of kinking is based on the reduced formulation, Equation (9b). This approach suppresses the oscillations by the $\varepsilon = 0$ assumption. Application of the full formulation, Equation (9a), requires selection of a length scale, l, often chosen as the face thickness, h_f, in sandwich debond analysis [5]. Figure 9 shows the phase angle for the original TSD specimen ($h_s = 0$) and a steel bar reinforced TSD specimen ($h_s = 12$ mm) (both with a H100 core) calculated using the full ($l = 2$ mm $= h_f$) and reduced formulations. It is observed that application of the full formulation ($l = 2$ mm) will shift the phase angle towards negative mode-mixities by about $25-30°$ depending on the tilt angle. The choice of the length scale must be consistent with experimental observations. One measure sensitive to the near-tip stress state is the angle at which a face/core crack would propagate, that is, the kinking angle. This suggests that
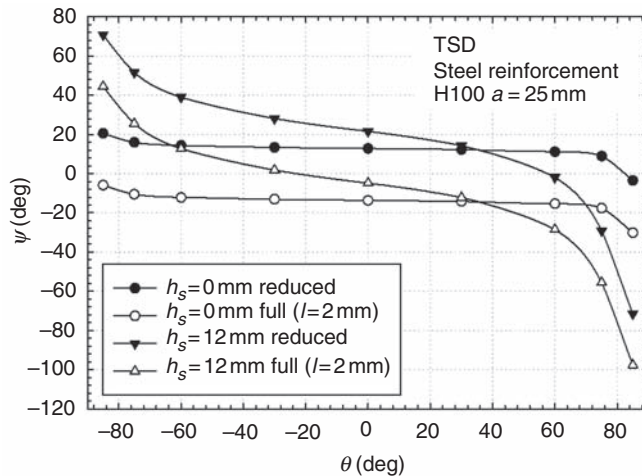
Figure 9. *Phase angle calculated using full and reduced formulations vs. tilt angle for original ($h_s = 0$ mm) and reinforced ($h_s = 12$ mm) TSD-specimens with a H100 25 mm core. $l = 2$ mm.*

experiments be conducted on TSD specimens where a failure mode transition occurs from face/core interface failure to crack kinking. Thus, in order to determine the length scale, l, in Equation (9a), l could be calibrated so that kinking sets in at a phase angle of $\psi_F = 0°$. This will be the subject of a later paper.

In order to investigate the response and mechanical behavior of the modified TSD-specimen when changing the crack length, and face and core stiffnesses and thicknesses, parametric analyses have been carried out as presented below.
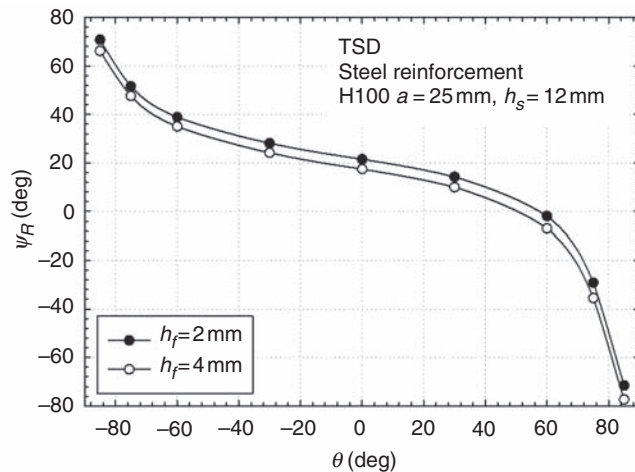
Effect of Crack Length

Figure 10 shows the phase angle (reduced formulation) as function of tilt angle for a steel reinforced ($h_s = 12$ mm) GFRP/H100 TSD specimen with 2 mm thick face sheets and 25 mm thick H100 core for crack lengths of 25–150 mm. As the crack length increases the relative shear contribution diminishes. As a consequence, the crack loading becomes more mode I dominated at longer crack lengths. This is in qualitative agreement with the results of Li and Thouless [14] who found a strong effect of crack length on their phase angle results.

Effect of Face Sheet Thickness and Material

TSD specimens with GFRP face sheets of thicknesses of 2 and 4 mm and a H100 core were considered ($a = 25$ mm). The steel reinforcement was 12 mm in both cases. Figure 11 shows the phase angle as a function of tilt angle for TSD specimens with the two face thicknesses. It can be observed that the face thickness has a small influence on the phase angle. This is expected since the 12 mm thick steel reinforcement will dominate the response of the specimen. Thus, it can be concluded that for the TSD specimen reinforced with a thick steel reinforcement, precise determination of face sheet thicknesses is not important.
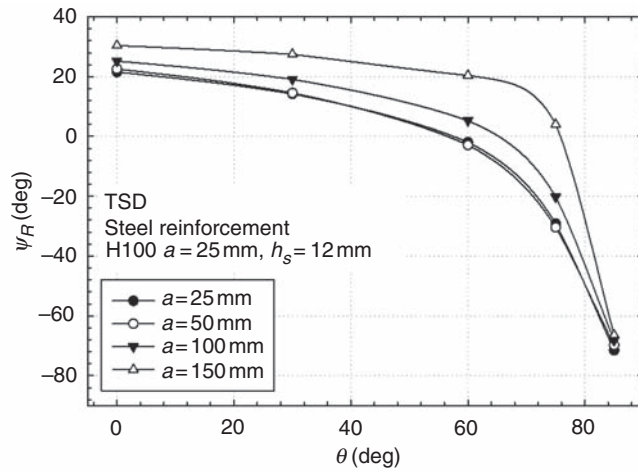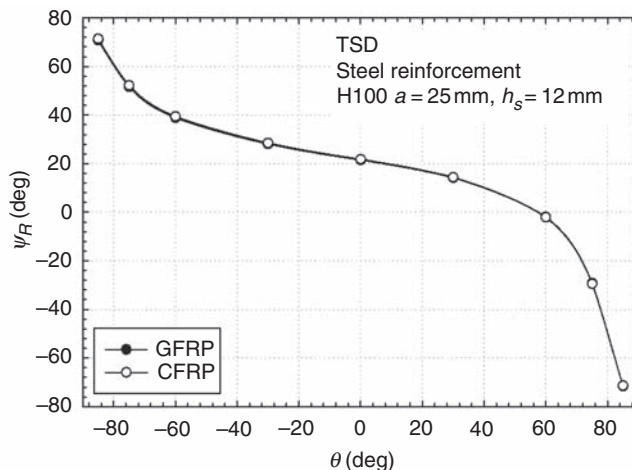
Figure 10. Phase angle (reduced formulation) vs. tilt angle for reinforced ($h_s = 12$ mm) GFRP/H100 TSD specimens with 2 mm face and 25 mm core thickness and a range of crack lengths, $a = 25–150$ mm.

Figure 11. Phase angle (reduced formulation) vs. tilt angle for a reinforced ($h_s = 12$ mm) GFRP/H100 TSD specimen with 25 mm crack length, 25 mm core thickness and face thicknesses of 2 and 4 mm.

The influence of face material on the phase angle is investigated for a TSD specimen with a 12 mm thick steel reinforcement and H100 core. The crack length was 25 mm and the face and core thicknesses were 2 and 25 mm, respectively. Typical material properties for GFRP and CFRP face sheets, see Table 2, were assumed. Results shown in Figure 12 verify that the face modulus has virtually no influence on the phase angle. It can be concluded as well that a precise measurement of the face sheet stiffness is not necessary for the modified TSD-specimen.

Figure 13 shows the influence of tilt angle on the applied load required to achieve $G = G_{IC}$ for a specimen with ($h_s = 12$ mm) with a H100 core with a 25 mm crack, 2 mm

Figure 12. *Phase angle (reduced formulation) vs. tilt angle for a reinforced ($h_s = 12$ mm) H100 TSD specimen with 25 mm crack length and 2 mm thick GFRP and CFRP faces and 25 mm thick core.*

thick face and 25 mm thick core. Both CFRP and GFRP faces (properties listed in Table 2) were examined. It can be observed that the applied load is increasing rapidly at larger tilt angles (and thus phase angles), as a result of the reduced contribution of mode I to the crack driving force and specimen compliance. Again it can be concluded from the results that the face sheet stiffness has no effect on the load level. However, regarding design of a suitable test setup, it is important to notice the increased load level for high tilt angles. Furthermore, the load levels presented in Figure 13 are given for a constant energy release rate of 400 J/m², typically measured as fracture toughness under mode I dominance. Thus, in actual testing considerably higher load levels can be expected for mode II dominated loading configurations based on earlier reported fracture toughness measurements in the literature [e.g., 5, 8, 13].

Effect of Core Thickness and Material

H100 core thicknesses in the range from 5 to 100 mm were examined. The steel reinforcement was 12 mm thick, the GFRP faces 2 mm thick and the crack length 25 mm. Figure 14 shows that reduced core thickness will reduce the phase angle at a given tilt angle. A reduced core thickness will promote localized shear deformation at the crack tip, thus resulting in more crack tip rotation.

The influence of core density on the phase angle (reduced formulation) was examined for a TSD specimen with a 12 mm steel reinforcement. The face and core thicknesses were 2 and 25 mm, and the crack length 25 mm. Furthermore, Dundur's parameter [17], α, given for isotropic materials in Equation (4) and for orthotropic materials in [19], for the three material configurations with GFRP faces and, respectively, H45, H100, and H200 cores was calculated to 0.993, 0.983, and 0.968. Figure 15 shows that the core density has small influence on the phase angle, which is in accordance with the small variation in α for the three material configurations. This indicates that geometry effects such as crack length dominate the variation in mode-mixity over core material choice for the investigated core material type and densities.
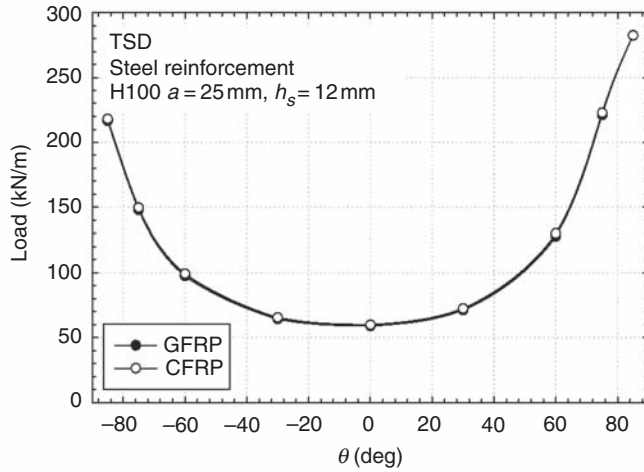
Figure 13. *Load required to achieve $G = G_{Ic}$ as function of tilt angle for a reinforced ($h_s = 12$ mm) H100 TSD specimen with 25 mm crack length, 2 mm face and 25 mm core thickness.*
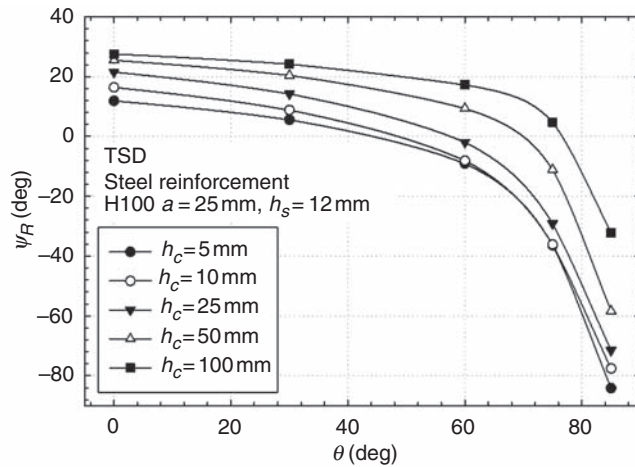
Figure 14. *Phase angle vs. tilt angle for face reinforced TSD specimens ($h_s = 12$ mm) with 25 mm crack length, 2 mm face thickness, and core thicknesses from 5 to 100 mm.*

Figure 16 shows the influence of core density on the load required to achieve $G = G_{IC}$. The required load increases substantially with increasing core density, and magnitude of phase angle.

FURTHER DESIGN MODIFICATIONS

As shown earlier, see Figures 7 and 14, the thicknesses of the steel reinforcement and the core largely influence the phase angle. It was shown that a small core thickness promoted
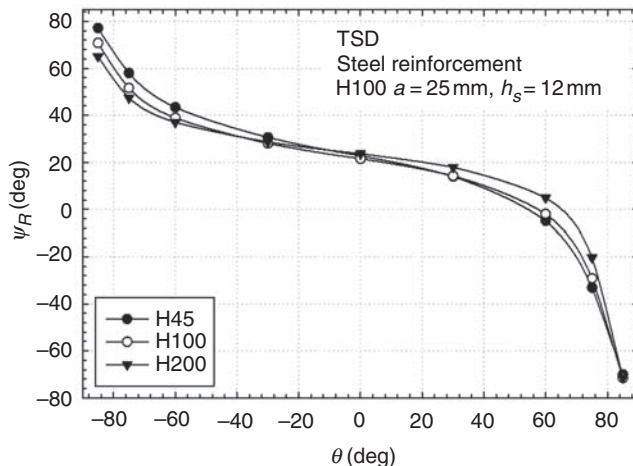
Figure 15. *Phase angle vs. tilt angle for face reinforced TSD specimens ($h_s = 12$ mm) with 25 mm crack length, 2 mm face, 25 mm core thickness, and three core densities.*
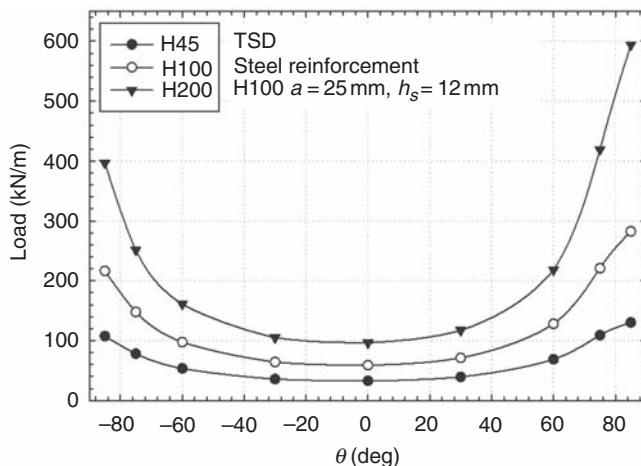

Figure 16. *Load required to achieve $G = G_{Ic}$ vs. tilt angle for a reinforced ($h_s = 12$ mm) GFRP TSD specimen with 25 mm crack length, 2 mm thick face sheets, and 25 mm thick H45, H100, and H200 cores.*

crack tip rotation and negative mode-mixity at large tilt angles. Global shear deformation of the core, at large tilt angles could also be reduced if the left edge of the TSD specimen is reinforced. To examine the influence of such a reinforcement, the action of such a reinforcement was simulated by fixing all DOF's of all nodes on the left edge of the specimen. Figure 17 shows phase angle vs. tilt angle for TSD specimens with a 25 mm thick H100 core and 2 mm thick face sheets with a 12 mm steel reinforcement at a crack length of 25 mm with and without such an end reinforcement. For larger tilt angles $\{20° < \theta < 85°\}$ the end reinforcement reduces the phase angle, apparently as a result of more localized shear deformation at the crack tip. Furthermore, Figure 18 shows contrary to the results
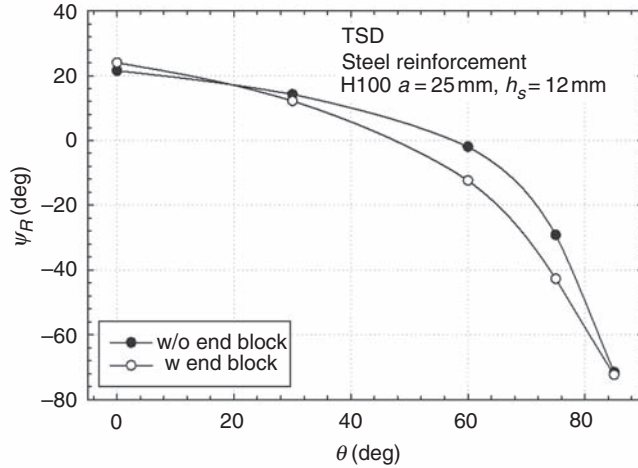
Figure 17. Phase angle (reduced formulation) vs. tilt angle for reinforced GFRP/H100 TSD specimens with 25 mm crack length, 2 mm face, and 25 mm core thicknesses with and without end block.
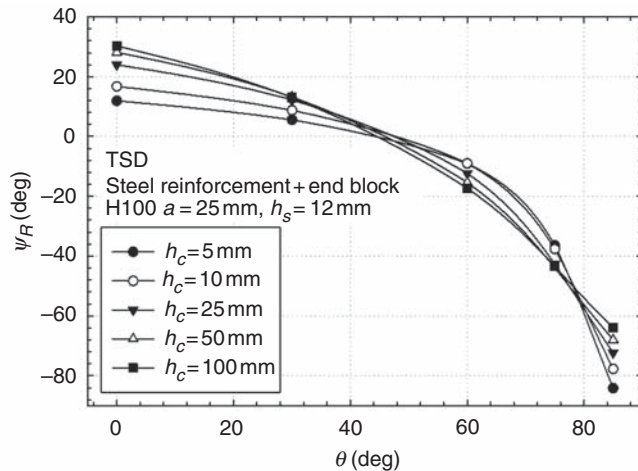
Figure 18. Phase angle (reduced formulation) vs. tilt angle for a reinforced ($h_s = 12$ mm) GFRP/H100 TSD specimen with 25 mm crack length and 2 mm face thickness with an end block and core thicknesses from 5 to 100 mm.

for the TSD specimen without the left end block reinforcement (Figure 14), that the relation between phase angle and tilt angle assumes close to a unique relation, independent of core thickness for larger core thicknesses. This indicates that the left block channels shear deformation to the crack tip region and causes crack tip rotation. For core thicknesses less that 10 mm, however, the phase angle vs. tilt angle relationship departs from the unique relation. It is believed that this behavior is due to the influence of the lower face sheet on the local crack tip deformation field.
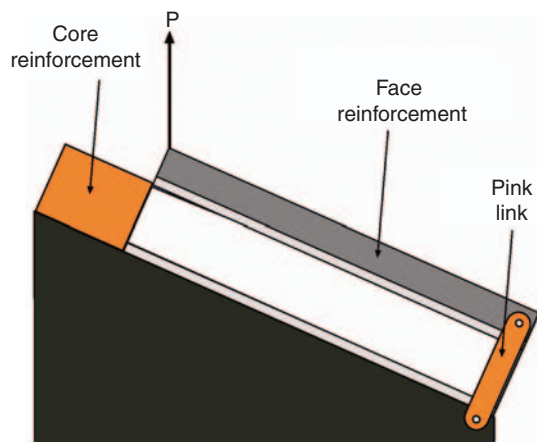
Figure 19. *Design modifications with pinned links at the specimen right end and a block, supporting the left end of the TSD specimen.*

It has been demonstrated that the end reinforcement of the left core edge could be a viable method to promote localized crack tip shear deformation. Such a method might be practically implemented by adhesively bonding or bolting a metal block to the base of the TSD fixture.

In the parametric analysis described above, the possibility for local failure of the TSD-specimen reinforced with a stiff steel bar was not considered. A potential failure site identified by the FEA stress results is yielding or failure in compression of the core at the right end of the reinforced specimen. Such stresses arise due to the necessity to maintain moment equilibrium during the almost rigid body rotation of the steel reinforced face sheet around the crack tip. Thus, when the steel reinforced specimen is loaded, the reinforced face sheet will rotate and the right end will have a tendency to indent into the core, possibly crushing the soft core material. Yielding or failure of the core violates the linear-elastic approach and must be avoided. To prevent core crushing without restricting shear deformation, a short link may be pin attached between the base of the fixture and the center of the steel reinforcement bar on both sides of the TSD specimen, see Figure 19. Also shown in Figure 19 is the earlier discussed end block reinforcement of the core.

Figure 20 shows the phase angle (reduced formulation) vs. tilt angle results for a TSD specimen with a H100 core and a 12 mm thick steel reinforcement, with a linkage at the right end, with and without the end block at lengths, $a = 25$, 50, 100, and 150 mm. Only positive tilt angles are considered. For crack lengths, $a = 25$ and 50 mm, comparison of the results for the reinforced and pinned configurations, Figure 20(a) and (b), show that the linkage has virtually no influence on the phase angle. The pinned link modification influences the phase angle results only for long crack lengths, Figure 20(c) and (d). At large tilt angles it is observed that the phase angle is approximately the same for all modification versions. It should be kept in mind, however, that the primary purpose of attaching the linkage at the right end of the specimen is to prevent core crushing, and based on the stress results (not shown) this objective has been satisfied.

In Figure 21 the phase angle is plotted vs. crack length for the *pinned* and *pinned + block* modifications of a steel reinforced ($h_s = 12$ mm) TSD specimen with 2 mm thick GFRP
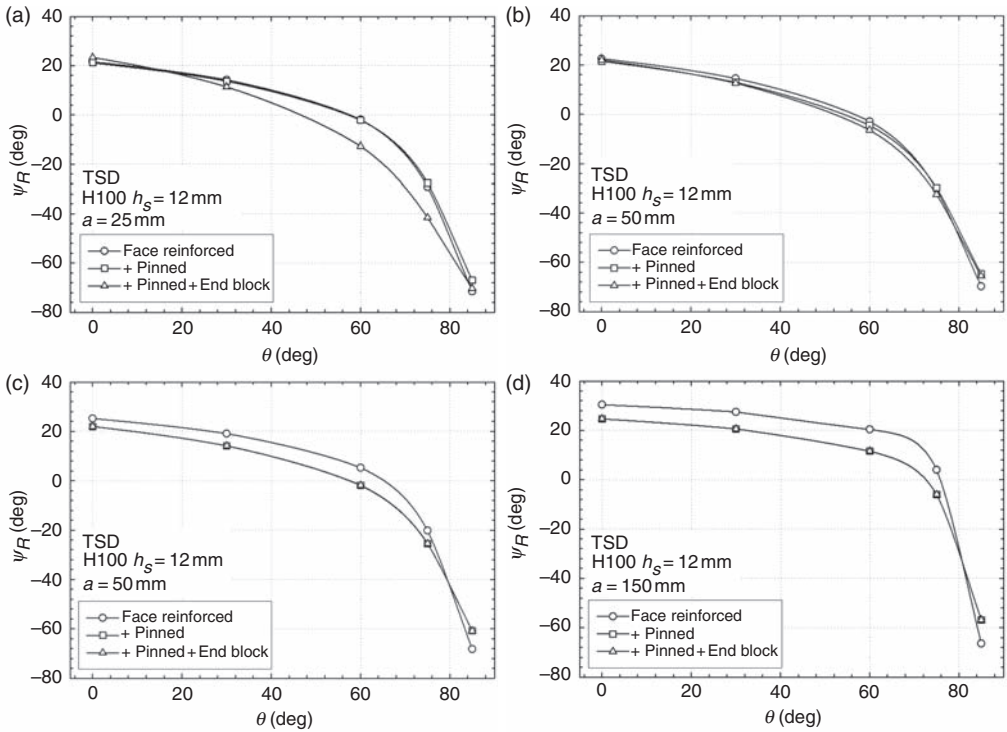
Figure 20. *Phase angle (reduced formulation) vs. tilt angle for the face reinforced, pinned, and pinned + block modification versions of reinforced TSD specimens with a H100 core. (a) $a = 25$ mm, (b) $a = 50$ mm, (c) $a = 100$ mm, and (d) $a = 150$ mm.*
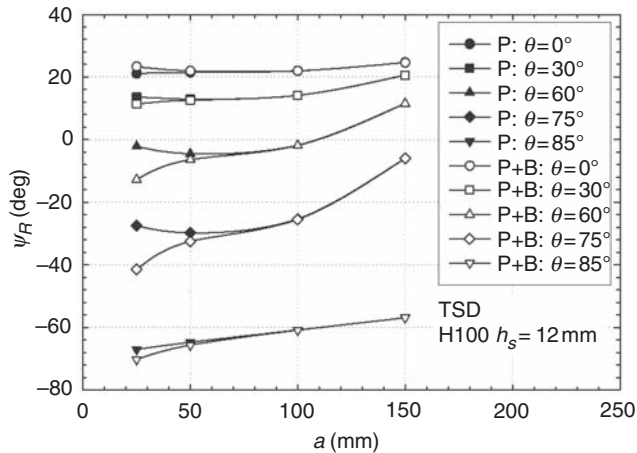
Figure 21. *Phase angle (reduced formulation) vs. crack length for the pinned and pinned + block modified versions of the TSD specimen with a H100 core. 'P' indicates the pinned version, and 'P + B' the pinned + block version.*

faces and a 25 mm thick H100 core. It is evident that the phase angle for the *pinned* version is approximately constant up to crack lengths of about 100 mm, where the phase angle increases significantly. For the *pinned + block* version the phase angle variation is more pronounced over the entire crack length regime, especially at larger tilt angles. Significant shear loading is achieved only at high tilt angles, where the sensitivity to changes of the tilt angle is high. This would increase the level of uncertainty in actual testing. This aspect must be kept in mind when conducting experimental studies with the reinforced TSD specimen especially in fatigue crack growth characterization, where the mode-mixity (phase angle) should not change as the crack grows longer.

Despite such limitations the results presented here illustrate that the modified TSD specimen should be viable for quasi-static mixed mode face/core interface fracture toughness measurements. The end *block* modification version was found to significantly extend the range of phase angles.

CONCLUSION

The finite element analysis of the original TSD specimen confirms the minor influence of tilt angle on the phase angle indicated by the Hutchinson–Suo analysis [16]. The range of mode-mixities for the TSD specimen, however, may be substantially expanded by reinforcing the loaded face sheet by a stiff metal bar. This leads to an increase in transverse shear and associated root rotation of the crack tip. The effect of such a reinforcement was most pronounced at short crack lengths. For typical face and core material combinations examined, the phase angle does not depend strongly on variations in face and core material properties. Further enhancement of crack tip shear loading was achieved by supporting the core at the cracked end of the specimen with a metal block. Core crushing at the un-cracked end of the specimen could be avoided by supporting the reinforced face sheet with stiff pinned links. For the investigated specimen geometry a steel reinforcement thickness of 12 mm of the face sheet was found to allow testing over a large range of the phase angles. Thus, the modified TSD specimen and test has been identified as a viable and promising candidate for mixed mode fracture toughness measurements of sandwich specimens with a soft core.

ACKNOWLEDGMENTS

REFERENCES

1. Li, X. and Carlsson, L.A. (1999). The Tilted Sandwich Debond (TSD) Specimen for Face/core Interface Fracture Characterization, *Journal of Sandwich Structures and Materials*, **1**: 60–75.
2. Li, X. and Carlsson, L.A. (2001). Fracture Mechanics Analysis of the Tilted Sandwich Debond (TSD) Specimen, *Journal of Composite Materials*, **35**(23): 2145–2168.

3. Prasad, S. and Carlsson, L.A. (1994). Debonding and Crack Kinking in Foam Core Sandwich Beams − I. Analysis of Fracture Specimens, *Engineering Fracture Mechanics*, **47**(6): 813–824.

4. Prasad, S. and Carlsson, L.A. (1994). Debonding and Crack Kinking in Foam Core Sandwich Beams − II. "Experimental Investigation, *Engineering Fracture Mechanics*, **47**(6): 825–841.

5. Berggreen, C., Simonsen, B.C. and Borum, K.K. (2007). Experimental and Numerical Study of Interface Crack Propagation in Foam Cored Sandwich Beams, *Journal of Composite Materials*, **41**(4): 493–520.

6. Lundsgaard-Larsen, C., Berggreen, C. and Carlsson, L.A. (2007). On The Use of a Woven Mat to Control The Crack Path in Composite Sandwich Specimens with Foam Core, In: *ASME International Mechanical Engineering Congress and Exposition*, 11–15 November, Seattle, WA.

7. Sørensen, B.F., Jørgensen, K., Jacobsen, T.K. and Østergaard, R.C. (2006). DBC Specimen Loaded with Uneven Bending Moments, *International Journal of Fracture*, **14**(1): 163–176.

8. Østergaard, R.C., Sørensen, B.F. and Brøndsted, P. (2007). Measurement of Interface Fracture Toughness of Sandwich Structures under Mixed Mode Loadings, *Journal of Sandwich Structures and Materials*, **9**: 445–466.

9. Lundsgaard-Larsen, C., Sørensen, B.F., Berggreen, C. and Østergaard, R.C. (2008). A Modified DCB Sandwich Specimen for Measuring Mixed Mode Cohesive Laws, *Engineering Fracture Mechanics*, **75**(8): 2514–2530.

10. Reeder, J. and Crews, J.H. (1990). Mixed-mode Bending Method for Delamination Testing, *AIAA Journal*, **28**(7): 1270–1276.

11. ASTM D6671/D 6671M-06 (2006). *Standard Test Method for Mixed Mode I−Mode II Interlaminar Fracture Toughness of Unidirectional Fiber Reinforced Polymer Matrix Composites*, ASTM International, Philadelphia, PA.

12. Quispitupa, A., Berggreen, C. and Carlsson, L.A. (2009). On the Analysis of a Mixed Mode Bending Sandwich Specimen for Debond Fracture Characterization, *Engineering Fracture Mechanics*, **76**(4): 594–613.

13. Quispitupa, A., Berggreen, C. and Carlsson, L.A. (2010). Design Analysis of the Mixed Mode Bending (MMB) Sandwich Specimen, *Journal of Sandwich Structures and Materials,* doi: 10.1177/1099636209104533.

14. Li, S., Wang, J. and Thouless, M.D. (2004). The Effects of Shear on Delamination in Layered Materials, *Journal of the Mechanics and Physics of Solids*, **52**: 193–214.

15. Ferrie, C.H., Sheinman, I. and Kardomateas, G.A. (1999). The Effect of Transverse Shear on the Postbuckling and Growth Characteristics of Delaminations in Composites, *Journal of Engineering Materials and Technology*, **121**(4): 406–412.

16. Hutchinson, J.W. and Suo, Z. (1992). Mixed Mode Cracking in Layered Materials, *Advances in Applied Mechanics*, **29**: 63–191.

17. Dundurs, J. (1969). Edge-bonded Dissimilar Orthogonal Elastic Wedges, *Journal of Applied Mechanics*, **36**: 630–652.

18. Viana, G.M. and Carlsson, L.A. (2002). Mechanical Properties and Fracture Characterization of Cross-linked PVC Foams, *Journal of Sandwich Structures and Materials*, **4**: 99–113.

19. Suo, Z. and Hutchinson, J.W. (1990). Interface Crack Between Two Elastic Layers, *International Journal of Fracture*, **43**(1): 1–18.